Batteries & Supercaps

Research Article
doi.org/10.1002/batt.202400428

Chemistry Europe
European Chemical Societies Publishing

www.batteries-supercaps.org

Sustainable Hard Carbon as Anode Materials for Na-Ion Batteries: From Laboratory to Upscaling

Zhenyu Guo,*[a] Kaitian Zheng,[a, b] Mengnan Wang,[a] Yichen Huang,[a] Yuanzhu Zhao,[a] Heather Au,[a] and Maria-Magdalena Titirici*[a, c]

Sodium-ion batteries (NIBs) are an alternative to lithium-ion batteries (LIBs), particularly in applications where cost, availability, and sustainability are more critical. Hard carbon is emerging as a promising anode material for NIBs, however, the scale up remains in developmental stages. In this study, we focus on the development and potential upscaling of sustainable hard carbon materials as anodes for NIBs. The synthesis of hard carbon starts from D-glucose, a scalable and environmentally benign precursor. A facile process combining hydrothermal carbonisation and subsequent pyrolysis at 1500 °C allows the hard carbon to become an industrially viable material. The resulting hard carbon demonstrates competitive performance metrics including a high initial Coulombic efficiency, high reversible capacity, long-term cycling stability, and rate capability. This study concludes with a discussion of the techno-economic analysis of adopting such sustainable materials in the battery industry, highlighting the potential for significant advancements in energy storage technologies.

Introduction

Lithium-ion batteries (LIBs) with graphite anodes have dominated the energy storage market for decades.[1] However, the recent surge in global demand for large-scale energy storage has raised concerns regarding the scarcity of critical resources used in LIBs and vulnerable value chains.[2] In Particular, lithium resources and graphite are only mined in limited geographical regions outside Europe.[3] In contrast, sodium is abundant and more readily accessible across Europe. The production of natural and synthetic graphite for battery use involves extensive mining and the carbonisation of petroleum products, respectively, both of which are energy-intensive processes with substantial environmental impacts.[4] These processes weaken the supply and value chains for the countries that are aiming to secure a stable, local supply of materials for battery production, to enhance energy security and sustainability.[5]

NIBs represent a more sustainable alternative, as they do not depend on critical materials, using instead abundant materials.[6] Similar to LIBs, NIBs operate based on the "rocking chair" mechanism, and they can be produced on almost the same production lines. This compatibility enables NIBs as a seamless "drop-in" technology.[7] Additionally, NIBs feature several performance advantages including high capacity,[8] high power density,[9] superior cycling performance,[6b,10] and excellent low-temperature performance.[11] Therefore, NIBs offer considerable potential not to replace but to supplement and enhance LIBs application, particularly in areas requiring high power and massive storage capacities where energy density is less critical.[12]

Regarding the anode side, unlike LIBs that require copper current collectors, NIBs use lighter and more abundant Al foil, enhancing the overall sustainability of the battery. However, due to thermodynamic reasons, a graphite anode is not compatible with ester-based electrolytes in NIBs. In 2000, hard carbon was reported to accommodate Na-ion.[13] Since then, hard carbon anodes have gained increasing popularity, and their promise as high-performing anodes in NIBs continues to grow.[6a] Despite the existing of many other types of anodes,[14] both academics and industrial stakeholders currently recognize hard carbon as the most promising anode for NIBs. More specifically, leading Na-ion battery companies such as Faradion, Tiamat, HiNa, CATL, and Northvolt, along with many research groups, present their practical cells using hard carbon as an anode, although cathode chemistry may vary.[6b,15] Nevertheless, hard carbon is characterised by a complicated structure with variations in surface area, degree of graphitisation, porosity, surface functionalities, etc. These characteristics are potential sites for Na-ion storage, meaning that not only individual structural motifs but their overall balance in the material control how Na-ion is stored. Hence it is crucial to study these materials extensively to understand the relationship between their structural features and performance.

[a] Z. Guo, K. Zheng, M. Wang, Y. Huang, Y. Zhao, H. Au, M.-M. Titirici
Department of Chemical Engineering, Imperial College London,London SW7 2AZ, UK
E-mail: z.guo19@imperial.ac.uk
m.titirici@imperial.ac.uk

[b] K. Zheng
Chemical Engineering Research Center, State Key Laboratory of Chemical Engineering, School of Chemical Engineering and Technology, Tianjin University, Tianjin 300072, China.

[c] M.-M. Titirici
Advanced Institute for Materials Research (WPI-AIMR), Tohoku University,2-1-1 Katahira, Aobaku, Sendai,Miyagi 980-8577,Japan
E-mail: m.titirici@imperial.ac.uk

Supporting information for this article is available on the WWW under https://doi.org/10.1002/batt.202400428

Research Article
doi.org/10.1002/batt.202400428
Chemistry Europe
European Chemical Societies Publishing

Recent lab-scale research has demonstrated the potential of hard carbon as an anode material for Na-ion batteries, but several challenges hinder its scale-up to meet industrial demands. Issues such as CO_2 emissions, environmental impacts, cost efficiency, and the need for comprehensive techno-economic and life cycle analyses are often overlooked in lab-scale studies. Industrially, the majority of hard carbon used in NIBs is sourced from the petroleum industry or through mining, both of which present environmental problems. Consequently, the large-scale production of NIBs is still far from reality, particularly within the EU, where it is challenging to meet the criteria set by the European Commission's European Green Deal, which mandates the sustainability of all batteries used within the EU.

This work presents our research group's effort in optimising hard carbon anodes for NIBs emphasising sustainability and high performance. Various perspectives are provided including material synthesis, structural characterisation, electrochemical studies in both coin cells and pouch cells, and techno-economic analysis (TEA). The hard carbons were synthesised via a hydrothermal carbonisation process with subsequent pyrolysis at 1500 °C. When used as an anode in NIBs, G1500 shows a high initial Coulombic efficiency of 91.67%, ultra-long cycling stability and a high energy density of up to 236 Wh kg^{-1}. Throughout this work, the potential commercialisation and challenges associated with hard carbon are discussed. Based on a large-scale model, we further conducted a TEA, which indicated that the glucose and HTC steps are two major contributors to this process.

Results and Discussion

Material Synthesis

Over the years, the Titirici group has been optimising hard carbon derived from HTC for use as an anode for various battery chemistries including Li-ion, Na-ion, and K-ion batteries.[10,16] In this work, an HTC carbon pyrolysed at 1500 °C (designated G1500) was used, having previously demonstrated superior electrochemical performance, particularly in terms of initial Coulombic efficiency, long cycling performance and rate performance. Consequently, G1500 is now considered one of the most promising candidates for further potential commercialisation. The synthesis route of G1500 is illustrated in Figure 1.

D-glucose (precursor) solution undergoes hydrothermal carbonisation, from room temperature to 230 °C, converting the glucose solution into a solid carbon-rich material (designated HTC carbon) under self-generated pressure. This procedure mimics the natural formation of coal but in an accelerated and controlled manner, allowing for precise tuning of the surface chemistry of the carbon.[17] Furthermore, the self-generated pressure of up to 45 bar pressure during hydrothermal carbonisation leads to a denser carbon material than that produced by conventional or direct pyrolysis.[18] Following HTC, the solid product is filtered and dried. The dried HTC carbon is then pyrolysed at 1500 °C under a N_2 atmosphere. This high-temperature pyrolysis is the key step to reduce oxygen content, control surface area, and increase the electrical conductivity of the carbon while maintaining a physically unchanged morphology. The resulting carbon is prepared for a slurry for battery use.

The HTC pretreatment is crucial for several reasons: firstly, the surface chemistry and structural features of the resulting carbon can be tuned by adjusting the precursor,[19] HTC additive,[16g] and HTC conditions.[20] Secondly, HTC-derived hard carbon outperformed the hard carbon derived via direct carbonisation of glucose powder in rate performance and reversible capacity.[16a] Thirdly, for high-quality battery-grade graphite, a spheroidisation step is crucial to homogenise the particle size and morphology to improve the packing density for enhanced volumetric capacities.[21] HTC intrinsically facilitates spherical primary particles of HTC carbon (Figure 2a) which not only suppress dendrite growth but also increase packing density.[16a] In the process, the use of glucose as the precursor aligns well with the European Union's strategic goals for sustainability and environmental responsibility. Glucose can

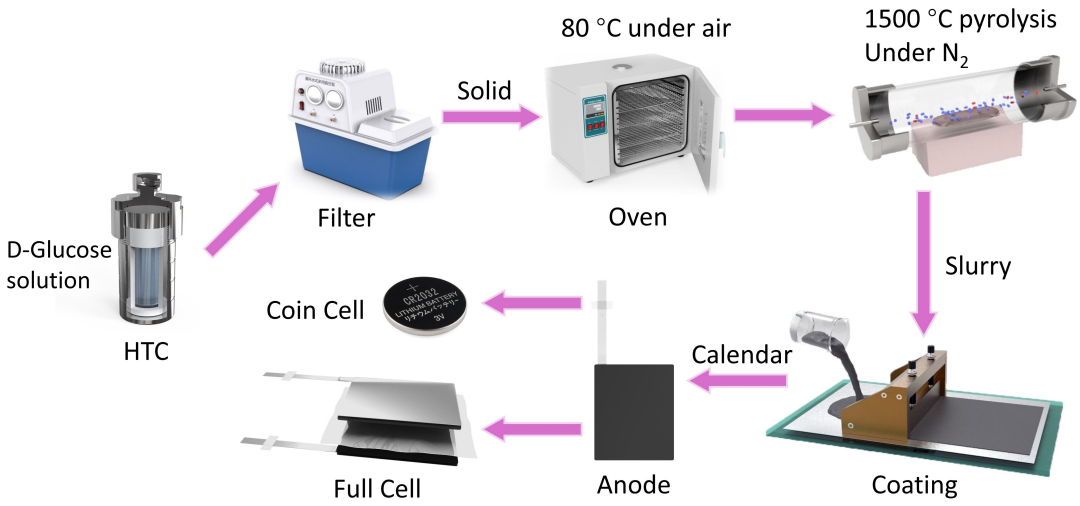

Figure 1. Overview of the current lab-scale flow from precursor to material to electrode to batteries.

Research Article
doi.org/10.1002/batt.202400428
Chemistry Europe
European Chemical Societies Publishing

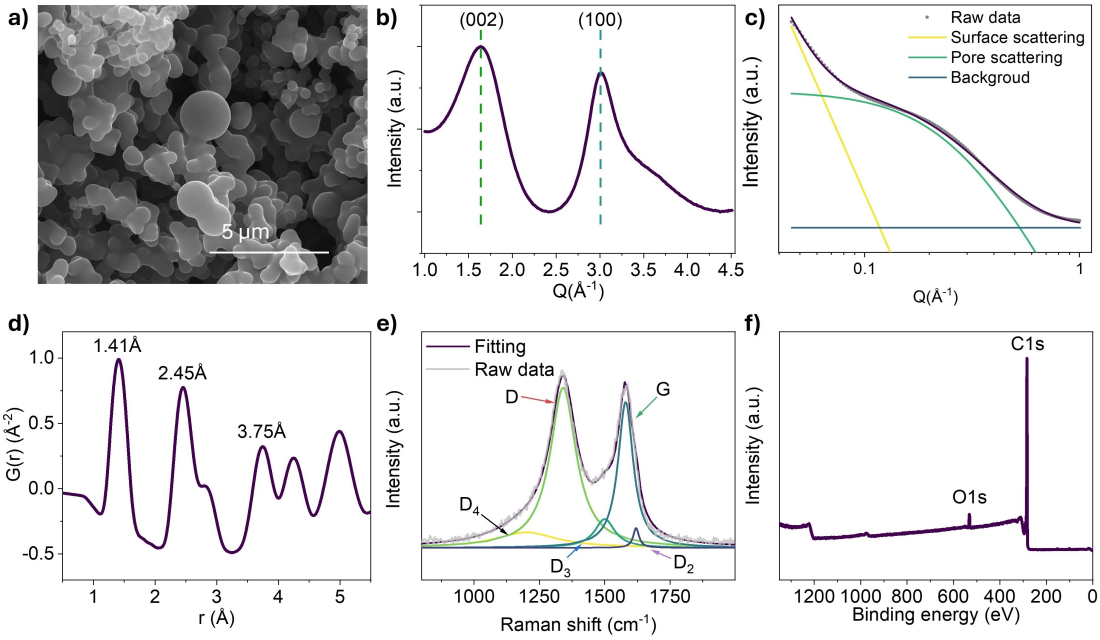

Figure 2. Structural characterisation of G1500: a) Scanning Electron Microscopy (SEM) image; b) Wide-angle neutron scattering (WANS) pattern; c) Small-angle X-ray neutron (SANS) pattern; d) Pair Distribution Function (PDF) analysis; e) Raman spectrum; f) X-ray Photoelectron Spectroscopy (XPS) survey spectrum.

be extracted from the breakdown of various biomass sources such as plants, agricultural waste, and other organic materials. Previous literature has discussed that glucose-derived hard carbon shows enhanced sustainability via life cycle analysis.[16a,e,22] Overall, the HTC pretreatment of glucose represents a promising approach that combines high performance with environmental practices. Such a synergy is crucial for developing NIB technologies in a sustainable manner.

The Structural Characterisation of G1500

In discussing the electrochemical sodiation mechanism of hard carbon anodes for NIBs, it is proposed that in the high voltage sloping region (>0.1 V vs. Na^+/Na), Na ions are adsorbed at carbon defects, onto pore surfaces and within large interlayers. The low-potential plateau region (<0.1 V vs. Na^+/Na) is due to the pore-filling mechanism forming metallic Na nanoclusters.[23] Hence, the micro-structure of hard carbon significantly influences the electrochemical performance of NIBs.

To investigate the morphology of G1500, scanning electron microscopy (SEM) images (Figure 2a, and Figure S1 in Supporting information) reveal a micro-sized, spherical morphology of the particles, with diameters ranging from 200 to 300 nm. Notably, those particles are aggregated together in a way that resembles a bunch of grapes. Each particle is closely packed with others yet retains a distinct spherical shape and boundary. This connection may have formed through physical adhesion during the hydrothermal carbonisation process, with subsequent pyrolysis having negligible impact on the overall morphology. This configuration facilitates dense packing of the particles, reducing surface area and thus the amount of electrolyte required to fully wet the electrode, which is beneficial for practical production. To further confirm this, measurements of the crystal density, size distribution and Brunauer-Emmett-Teller (BET) surface area were conducted (Figure S2 in Supporting information). Particle size analysis indicates that 10%, 50%, and 90% of the hard carbon particles are smaller than 2.40 μm, 9.97 μm (median particle size) and 29.23 μm, respectively. Although the individual particles are sub-micron in size, the aggregated form results in large particles with a relatively low surface area of 11 $m^2 g^{-1}$ and a high crystal density of 1.73 g cm^{-3}, as determined by nitrogen adsorption analysis and crystal density. When compared to commercial graphite, which typically has a particle size of 8–30 um and a low surface area of up to 8 $m^2 g^{-1}$,[1b,24] G1500 shows the potential for commercial scalability from the perspective of similar morphology.

Structural analysis of the bulk material G1500 with wide-angle neutron scattering (WANS) (Figure 2b) shows (002) and (100) peaks. From the position of the (002) peak, an average d-spacing of 3.83 Å can be obtained. Due to the pore-filling mechanism dominating the plateau capacity, the pore size becomes an important parameter. Based on the assumption that the closed pores of G1500 are spherical, the fitted SANS pattern (Figure 2c) indicates that the average closed pore size is *ca.* 2.3 nm in diameter. This pore size aligns well with the literature-reported size range of 13–15 Å for Na nanoclusters.[25] This match in size suggests a suitable structural fit for Na-ion storage. Pair distribution function (PDF) analysis provides additional insights into the atomic arrangement within G1500. From Figure 2d and Figure S3 (Supporting information), the first peak at 1.41 Å corresponds to the nearest neighbour C–C bond distance indicating the presence of 6-membered carbon rings

(hexagonal rings). The second peak at 2.45 Å corresponds to the next-nearest C–C distance, characteristic of the hexagonal lattice in graphene-like structures.

Apart from the graphitic structure, the defect concentration plays an important role in high-performance NIBs.[26] G1500 shows a moderate level of defects with an ID/IG value of 1.10 from Raman spectroscopy (Figure 2e), compared to other hard carbon.[16c] When it comes to surface chemistry, due to the use of pure glucose, only carbon and oxygen of *ca.* 3.7 at. % can be detected from XPS analysis (in Figure 2f). The detailed fine scans of O1s and C1s of G1500 were shown in Figure S4 in Supporting information. The parameters of G1500 are summarised below in Table 1.

The Electrochemistry of G1500 Anode

In electrochemical studies, Figure 3a shows the first three charge-discharge cycles of G1500 in a half cell (coin cell) at a current density of 30 mA g^{-1}, with a high initial Coulombic efficiency of 91.67%. G1500 typically has an initial Coulombic efficiency (ICE) of 91.0%–92.6% in half-cell configuration with electrolytes of 1.0 M $NaPF_6$ in EC and DEC solvent mix (1: 1 in volume) without any additives. Cyclic voltammetry curves (Figure 3c) also show little variation over the first few cycles. For practical cells, one of the most crucial parameters is the ICE. With a high ICE, the energy density can be enhanced by reducing the amount of cathode to compensate for irreversibility during the first few cycles, also lowering the cell manufacturing costs and improving cell formation efficiency. As a benchmark, high-quality commercial graphite anodes in LIBs typically exhibit an ICE of 90 – 96%.[24] The high ICE observed in pyrolysed HTC carbons has been reported previously.[27] The study indicated that pyrolysed HTC-derived carbon dots exhibit unique surface chemistry with an enhanced ICE. Hence the unique nanosized carbon dots stabilise the surface chemistry to reduce irreversible loss during SEI formation. Such a phenomenon could be one reason that contributes to G1500 having one of the highest ICE values reported for hard carbon anodes in NIBs without pre-sodiation.[28]

Figure 3b illustrates more clearly that the plateau region of both the charging and discharging processes occur between 0 and 0.1 V vs. Na^+/Na as evidenced by the peaks in the dQ dV^{-1} plot. This is beneficial since a lower de-sodiation potential in a half cell leads to a higher discharge energy density in a full cell. Moreover, the small voltage hysteresis between the sodiation and de-sodiation potential means more of the energy used during charging will be available during discharge enhancing the overall energy efficiency. In a full cell (pouch cell), when paired with a $Na_3V_2(PO_4)_3$ (NVP) cathode, the charge-discharge curve of the first cycle of the full cell shows a high initial Coulombic efficiency of 90.68%, as shown in Figure 3d. These results are comparable to typical ICE of 85–92% in commercial LIBs.[29]

Long-term cycling of the two pouch cells with a configuration of G1500|1 M $NaPF_6$ in EC DEC|NVP at 0.3 A g^{-1} was conducted. After 5100 cycles and 4300 cycles, two pouch cells still show retention rates of over 88% and over 91%, demonstrating the practicality of G1500 in long-term storage systems. In selecting NVP as the cathode material for this study, NVP is characterised by its structural stability during the insertion and extraction of Na ions, which is crucial for long-term cycling.[30] Prolonging battery lifetime offsets the environmental cost of using NVP. While vanadium is recognised as a critical material, which could potentially complicate supply chain sustainability, our research team is actively addressing this challenge. We are in the process of developing and patenting recycling methods for vanadium from spent NVP. This approach not only mitigates the environmental and economic concerns associated with the use of critical materials but also aligns with global sustainability goals.

It is important to note that lab conditions, such as the testing protocols, and monolayer versus multilayer pouch cells, may differ from industrial standards, but the results still show potential for commercial application. We further extended from half-cell coin cells and two electrode pouch cells to 3-electrode pouch cells to measure the specific capacity of G1500.

Rate Performance of G1500 Measured in Three-Electrode Configuration

It is documented that the specific capacity of hard carbon measured in a half cell can be significantly underestimated particularly when using large current density, or when using ester-based electrolytes. This inaccuracy comes from the increased polarisation caused by the high stripping potential of sodium metal, which can distort capacity measurements.[31] In a two-electrode coin cell system, the Na metal is used also as the reference electrode, causing the system to reach the cut-off voltage prematurely when the depth of the sodiation is not 100%. Typically, there are two ways to mitigate the effect of the

Table 1. Structure parameters of G1500.

	d_{002}[a] (Å)	$FWHM_{002}$[a] (A^{-1})	I_D/I_G	S_{BET}[b] (m^2 g^{-1})	D[c](nm)	C at. %
G1500	3.83	0.55	1.10	11	2.29	96.7
	Crystal Density (g cm^{-3})	**Tap Density (g cm^{-3})**	**Primary size (nm)**	**D_{10} (μm)**	**D_{50}(μm)**	**D_{90}(μm)**
G1500	1.73	0.7–0.9	200–300	2.40	9.97	29.23

[a] Calculated from WANS data.
[b] Surface area using the Brunauer-Emmett-Teller (BET) method.
[c] Pore diameter calculated from SANS.

Research Article
doi.org/10.1002/batt.202400428
Chemistry Europe
European Chemical Societies Publishing

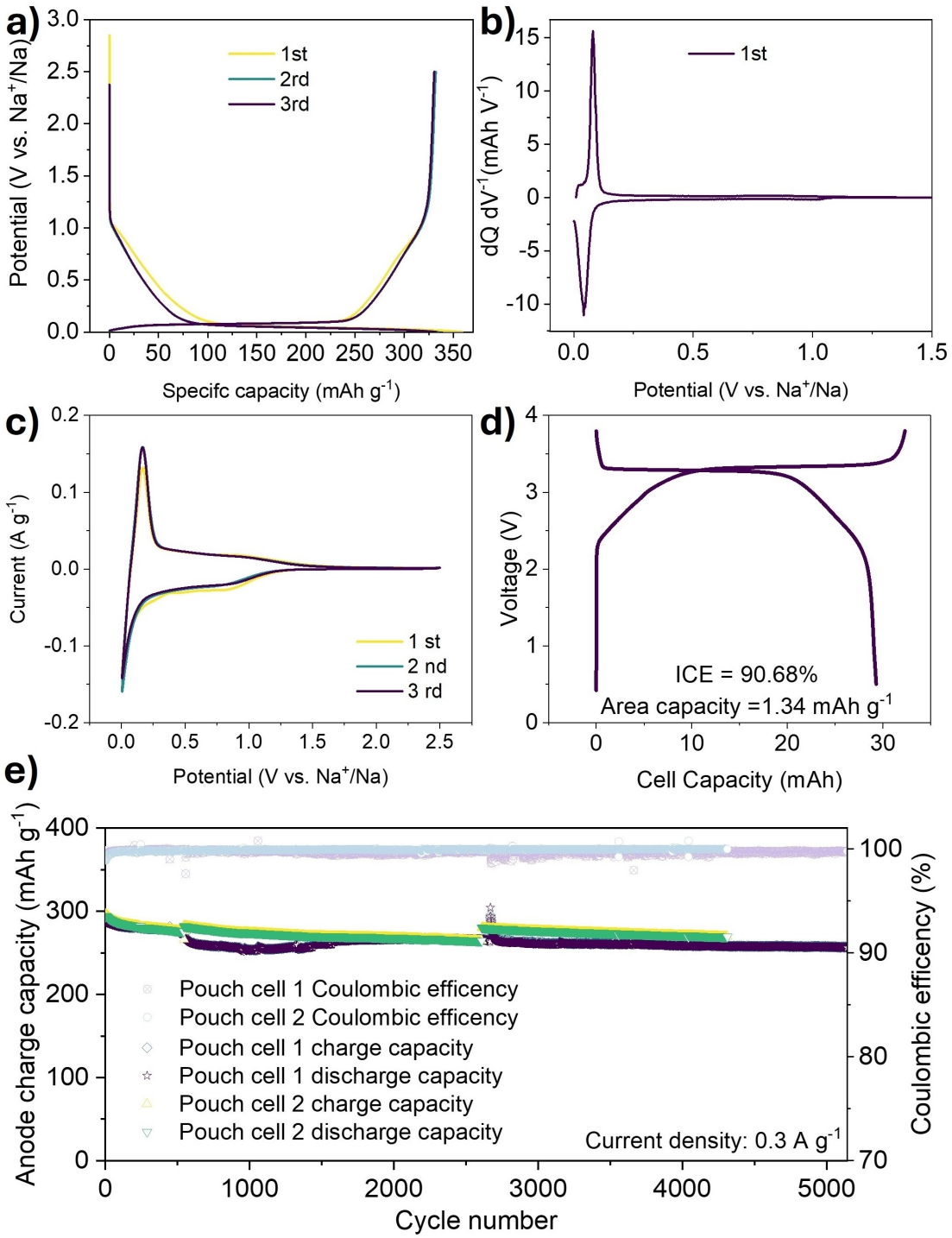

Figure 3. a) The first three galvanostatic charge-discharge cycles of G1500 anode in half cell at a current density of 30 mA g^{-1} with a high initial Coulombic efficiency of 91.67%; b) 1st cycle differential capacity plot (dQ dV^{-1} curve) of G1500 half-cell; c) cyclic voltammetry curves of the first three cycles of G1500 in half-cell; d) the 1st galvanostatic charge-discharge profile of a full cell with a configuration of G1500 | 1M $NaPF_6$ in EC DEC | $Na_3V_2(PO_4)_3$; e) the ultra-long cycling performance of two monolayer pouch cells with the same configuration of G1500 | 1M $NaPF_6$ in EC DEC | $Na_3V_2(PO_4)_3$ (the discontinuities in the cycling performance was mainly caused by power cuts etc).

polarised Na metal: (a) instead of using an ester-based electrolyte, using an ether-based electrolyte (e.g., 1 M $NaPF_6$ in diglyme) with a small polarisation; (b) using a three-electrode configuration to measure the intrinsic specific capacity of a hard carbon. The concerns associated with the former solution are that the different electrolytes decompose into different SEI and CEI layers both in thickness and composition on Na metal and hard carbon, leading to different diffusivity/resistance; the mechanisms of Na-ion storage in hard carbon can vary in different electrolytes, a subject which has been long debated.

Research Article
doi.org/10.1002/batt.202400428
Chemistry Europe
European Chemical Societies Publishing

To accurately measure the specific capacity of G1500, herein we used a three-electrode pouch cell (Figure 4a) with Na metal as the reference electrode, NVP as the cathode, 1 M $NaPF_6$ in EC: DEC as the electrolyte and the hard carbon G1500 as the anode.

Figure 4b demonstrates that the G1500 | 1 M $NaPF_6$ in EC: DEC | NVP pouch cell delivered high rate performance, achieving 213 mAh g^{-1} at a current density of 3 A g^{-1} and 311 mAh g^{-1} at 30 mA g^{-1}. Figure 4c and Figure 4d illustrate how the voltage changes during testing, and the growing overpotential with current density in both electrodes is still observed. It is noted that at a high current, the hard carbon cannot reach the cut-off during de-sodiation. This pouch cell delivered a high energy density of 230.8 Wh kg^{-1} at a power density of 22.3 W kg^{-1}, and a high power density of 1971.6 W kg^{-1} at 140.2 Wh kg^{-1}. The mass loading of this pouch cell is 4.3 mg cm^{-2} of G1500 and 13.73 mg cm^{-2} of NVP, the areal capacity is 1.34 mAh cm^{-2}. The areal capacity ratio of the hard carbon to the NVP (N/P ratio) is 1.05 with G1500. This experiment provides practical insights into the performance of hard carbon in a realistic N/P ratio setting and its operational characteristics in NIBs.

Techno-Economic Analysis of G1500

Based on the promising electrochemical performance and previous life cycle analysis,[16a,e, 22] we further conducted a techno-economic analysis (TEA) to evaluate the economic viability of the G1500 hard carbon production process. This TEA, based on data from a UK production scale of 50 kg per hour, aims to de-risk the process by evaluating its cost-effectiveness at technology readiness levels 3–4. The analysis, while preliminary and subject to adjustments based on location and specific synthesis conditions, provides essential economic insights. Further details and modelling parameters are available in the supplementary information.

As illustrated in Figure 5, in the development of G1500 hard carbon, the production process begins with hydrothermal carbonisation (HTC), followed by filtering, drying, and concludes with carbonisation. The mass balance calculations were initially performed on a laboratory scale with 5 g per batch, and subsequently scaled up linearly for broader application. The capital and operational costs for this process, informed by the latest data from Sinnott and Towler's "Chemical Engineering Design" (Elsevier, 2019),[32] are detailed in the inventory raw data sheet.

Our analysis reveals that the net production cost (NPC) of G1500 is approximately $7.5 per kg (as shown in Figure 6),

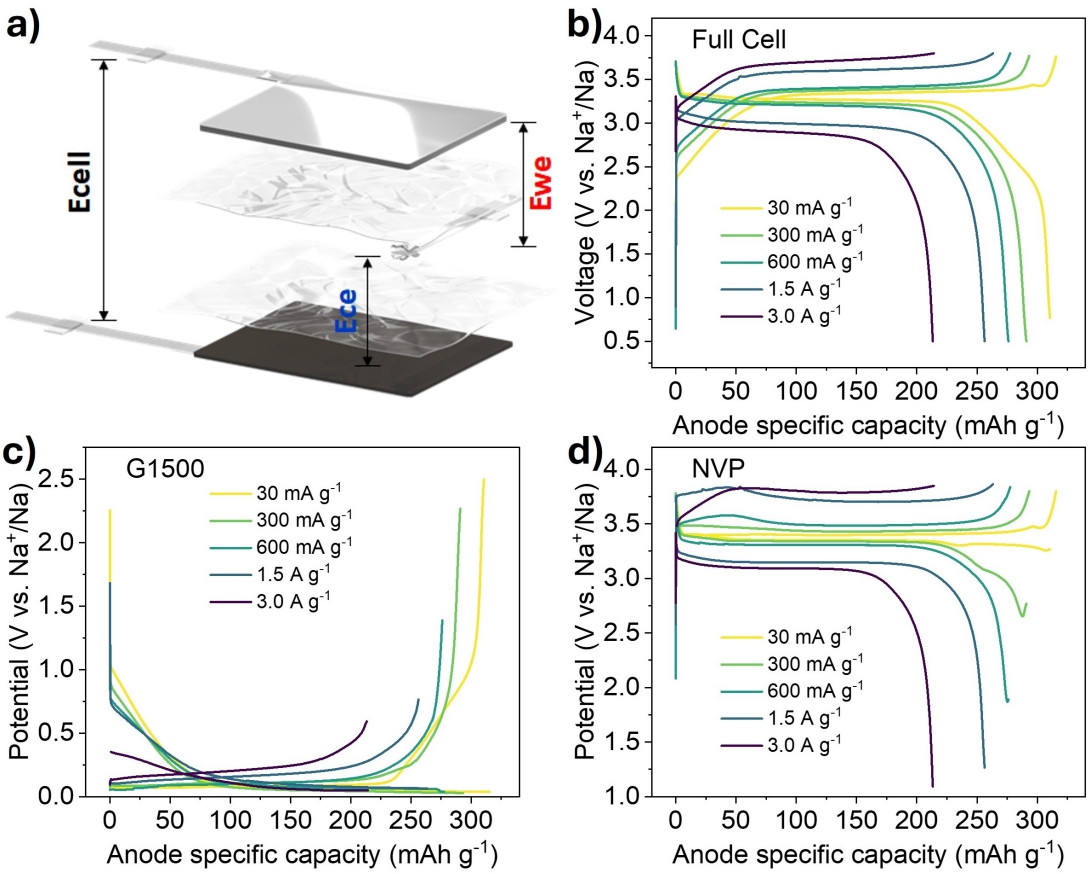

Figure 4. a) Schematic illustration of the 3-electrode pouch cell. The galvanostatic charge-discharge profiles at different current densities of a pouch cell G1500 | 1M $NaPF_6$ in EC: DEC (1 : 1 in v.) | NVP using a three-electrode configuration with a Na metal as the reference: a) schematic diagram; b) G1500 vs NVP, c) G1500 vs Na reference; d) NVP vs Na reference. The current density and the specific capacity were both calculated based on the mass of G1500.

Research Article
doi.org/10.1002/batt.202400428
Chemistry Europe
European Chemical Societies Publishing

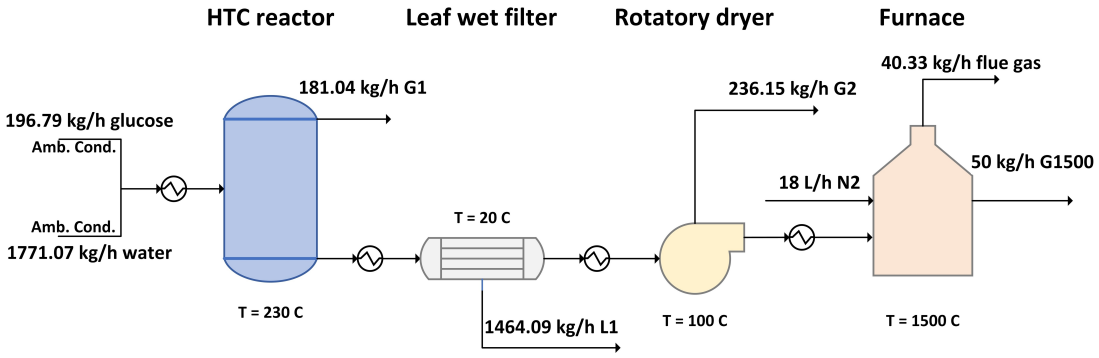

Figure 5. Process flow diagram to produce G1500 at a rate of 50 kg per hour.

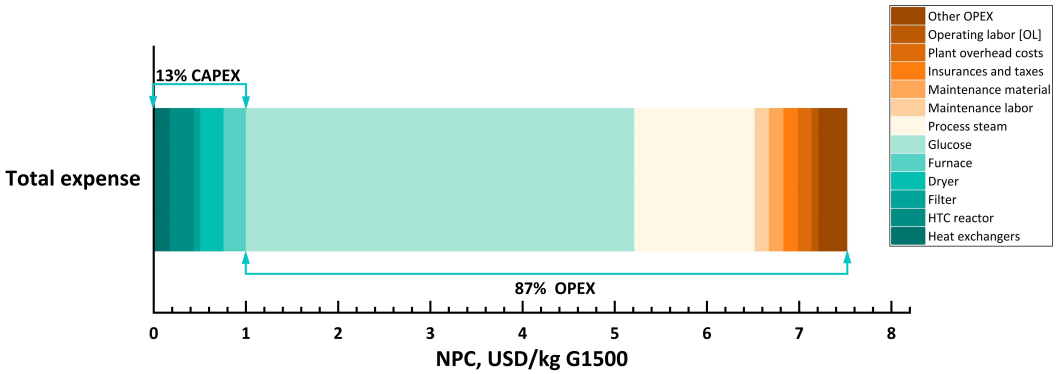

Figure 6. The breakdown of net production costs highlights major contributions from precursor procurement and steam for HTC heating.

which is competitive within the market range of $7 to $15 per kg. A comparison table (Table S1 in Supporting information) summarises synthesis methods on hard carbons. More importantly, the major cost drivers were identified as the precursor (industrial grade glucose) at 56% and heating at 17%, with over 90% of the heating costs attributable to the HTC process alone. This result is contrary to common assumptions that pyrolysis, requiring high temperatures, would be the most expensive heating phase. Instead, the extended duration and volume required for the HTC step incur the majority of these costs. Future sensitivity analysis (Figure S1) also indicates that alterations in precursor usage and optimization of the HTC operations could lead to significant reductions in production costs.

Conclusions

In summary, this work has presented the sustainable hard carbon G1500 as a commercially viable anode for NIBs, through a facile synthesis process combining hydrothermal carbonization and subsequent pyrolysis at 1500 °C. This process allows for potential scaling up of production. G1500 demonstrates a high initial Coulombic efficiency of 91.67%, a high reversible capacity of 330–340 mAh g^{-1}, a high energy density of 236 Wh kg^{-1} at a power density of 22.3 W kg^{-1} (based on the mass of anode and cathode only), and a high power density of 1971.6 W kg^{-1} at 140.2 Wh kg^{-1}, stable cycling stability, and rate capability. Those metrics are promising for developing G1500 towards commercialisation. A comprehensive techno-economic analysis indicates the hard carbon's competitive price; however, it also highlights the two major cost contributors: glucose and high-temperature steam required for hydrothermal carbonisation.

Acknowledgements

This work is supported by funding grants from RAEng CiET (1819\2\60), Faraday Institution (NEXGENNA, FIRG064), the Engineering and Physical Sciences Research Council (EP/R021554/2, EP/S018204/2), the Imperial College London DT prime commercialisation project, and the Imperial College London Seed fund.

Conflict of Interests

The authors declare no conflict of interest.

Data Availability Statement

The data that support the findings of this study are available from the corresponding author upon reasonable request.

Keywords: Hard carbon · Sodium-ion batteries · Full cells · Three-electrode system · Techno-economic analysis

[1] a) M. Li, J. Lu, Z. Chen, K. Amine, *Adv. Mater.* **2018**, *30*, e1800561; b) Y. Nishi, *Chem. Rec.* **2001**, *1*, 406–413.
[2] M.-M. Titirici, A. Chitre, D. Freake, L. Lander, J. Edge, *Batteries Supercapsp.* **2020**, *3*, 1126.
[3] S. Bobba, S. Carrara, J. Huisman, F. Mathieux,, C. Pavel, European Commission, *Critical Raw Materials for Strategic Technologies and Sectors in the EU—A Foresight Study*, Publications Office of the European Union: Luxembourg, 2020. [Online]. Available: https://www.europeansources.info/record/critical-raw-materials-for-strategic-technologies-and-sectors-in-the-eu-a-foresight-study/. [Accessed: October 15, 2023).
[4] L. Zhao, B. Ding, X. Y. Qin, Z. Wang, W. Lv, Y. B. He, Q. H. Yang, F. Kang, *Adv. Mater.* **2022**, *34*, 2106704.
[5] J. Husmann, J.-L. Popien, F. Cerdas, A. Barke, T. S. Spengler, C. Herrmann, *Procedia CIRP* **2024**, *122*, 121–126.
[6] a) Y. Gao, H. Zhang, J. Peng, L. Li, Y. Xiao, L. Li, Y. Liu, Y. Qiao, S. L. Chou, *Carbon Energy* **2024**, e464; b) A. Rudola, R. Sayers, C. J. Wright, J. Barker, *Nat. Energy* **2023**, *8*, 215–218.
[7] a) M. D. Slater, D. Kim, E. Lee, C. S. Johnson, *Adv. Funct. Mater.* **2013**, *23*, 947–958; b) K. Chayambuka, G. Mulder, D. L. Danilov, P. H. Notten, *Adv. Energy Mater.* **2020**, *10*, 2001310.
[8] A. Kamiyama, K. Kubota, D. Igarashi, Y. Youn, Y. Tateyama, H. Ando, K. Gotoh, S. Komaba, *Angew. Chem. Int. Ed. Engl.* **2021**, *60*, 5114–5120.
[9] a) Y. Li, A. Vasileiadis, Q. Zhou, Y. Lu, Q. Meng, Y. Li, P. Ombrini, J. Zhao, Z. Chen, Y. Niu, *Nat. Energy* **2024**, *9*, 134–142; b) A. Rudola, C. J. Wright, J. Barker, *J. Electrochem. Soc.* **2021**, *168*, 110534.
[10] Z. Guo, Z. Xu, F. Xie, J. Jiang, K. Zheng, S. Alabidun, M. Crespo-Ribadeneyra, Y. S. Hu, H. Au, M. M. Titirici, *Adv. Mater.* **2023**, *35*, 2304091.
[11] C. Che, F. Wu, Y. Li, Y. Li, S. Li, C. Wu, Y. Bai, *Adv. Mater.* **2024**, *36*, 2402291.
[12] J.-M. Tarascon, *Joule* **2020**, *4*, 1616–1620.
[13] J. R. Dahn, J. A. Seel, *J. Electrochem. Soc.* **2000**, *147*, 899–901.
[14] N. Tapia-Ruiz, A. R. Armstrong, H. Alptekin, M. A. Amores, H. Au, J. Barker, R. Boston, W. R. Brant, J. M. Brittain, Y. Chen, M. Chhowalla, Y.-S. Choi, S. I. R. Costa, M. Crespo Ribadeneyra, S. A. Cussen, E. J. Cussen, W. I. F. David, A. V. Desai, S. A. M. Dickson, E. I. Eweka, J. D. Forero-Saboya, C. P. Grey, J. M. Griffin, P. Gross, X. Hua, J. T. S. Irvine, P. Johansson, M. O. Jones, M. Karlsmo, E. Kendrick, E. Kim, O. V. Kolosov, Z. Li, S. F. L. Mertens, R. Mogensen, L. Monconduit, R. E. Morris, A. J. Naylor, S. Nikman, C. A. O'Keefe, D. M. C. Ould, R. G. Palgrave, P. Poizot, A. Ponrouch, S. Renault, E. M. Reynolds, A. Rudola, R. Sayers, D. O. Scanlon, S. Sen, V. R. Seymour, B. Silván, M. T. Sougrati, L. Stievano, G. S. Stone, C. I. Thomas, M.-M. Titirici, J. Tong, T. J. Wood, D. S. Wright, R. Younesi, *JPhys Energy* **2021**, *3*, 031503.
[15] a) N. LeGe, X.-X. He, Y.-X. Wang, Y. Lei, Y.-X. Yang, J.-T. Xu, M. Liu, X. Wu, W.-H. Lai, S.-L. Chou, *Energy Environ. Sci.* **2023**, *16*, 5688–5720; b) C. Wu, Y. Yang, Y. Zhang, H. Xu, X. He, X. Wu, S. Chou, *Chem. Sci.* **2024**, *15*, 6244–6268; c) F. Xie, Z. Xu, G. Zhenyu, M.-M. Titirici, *Prog. Energy* **2020**, *2*, 042002.
[16] a) Z. Xu, J. Wang, Z. Guo, F. Xie, H. Liu, H. Yadegari, M. Tebyetekerwa, M. P. Ryan, Y. S. Hu, M. M. Titirici, *Adv. Energy Mater.* **2022**, *12*, 2200208; b) H. Alptekin, H. Au, E. Olsson, J. Cottom, A. C. S. Jensen, T. F. Headen, Q. Cai, A. J. Drew, M. Crespo Ribadeneyra, M.-M. Titirici, *Adv. Mater. Interfaces* **2021**, *9*, 2101267; c) H. Au, H. Alptekin, A. C. S. Jensen, E. Olsson, C. A. O'Keefe, T. Smith, M. Crespo-Ribadeneyra, T. F. Headen, C. P. Grey, Q. Cai, A. J. Drew, M.-M. Titirici, *Energy Environ. Sci.* **2020**, *13*, 3469; d) E. Olsson, J. Cottom, H. Au, M.-M. Titirici, Q. Cai, *Carbon* **2021**, *177*, 226–243; e) H. Liu, Z. Xu, Z. Guo, J. Feng, H. Li, T. Qiu, M.-M. Titirici, *Philos. Trans. R. Soc. London Ser. A* **2021**, *379*, 20200340; f) E. Olsson, J. Cottom, H. Au, Z. Guo, A. C. S. Jensen, H. Alptekin, A. J. Drew, M.-M. Titirici, Q. Cai, *Adv. Funct. Mater.* **2020**, *30*, 1908209; g) H. Alptekin, H. Au, A. C. Jensen, E. Olsson, M. Goktas, T. F. Headen, P. Adelhelm, Q. Cai, A. J. Drew, M.-M. Titirici, *ACS Appl. Energ. Mater.* **2020**, *3*, 9918.
[17] M.-M. Titirici, R. J. White, C. Falco, M. Sevilla, *Energy Environ. Sci.* **2012**, *5*, 6796–6822.
[18] M. M. Titirici, A. Thomas, S.-H. Yu, J.-O. Müller, M. Antonietti, *Chem. Mater.* **2007**, *19*, 4205–4212.
[19] F. Xie, Z. Xu, A. Jensen, F. Ding, H. Au, J. Feng, H. Luo, M. Qiao, Z. Guo, Y. Lu, A. Drew, Y.-S. Hu, M.-M. Titirici, *J. Mater. Chem. A* **2019**, *7*, 27567.
[20] G. P. Lakienko, Z. V. Bobyleva, V. Gorshkov, A. I. Zybina, O. A. Drozhzhin, A. M. Abakumov, E. V. Antipov, *J. Electrochem. Soc.* **2024**, *171*, 060512.
[21] B. Biber, S. Sander, J. Martin, M. Wohlfahrt-Mehrens, M. Mancini, *Carbon* **2023**, *201*, 847–855.
[22] F. Trotta, G. J. Wang, Z. Guo, Z. Xu, M. Crespo Ribadeneyra, H. Au, J. S. Edge, M.-M. Titirici, L. Lander, *Adv. Sustainable Syst.* **2022**, *6*, 2200047.
[23] a) J. Yang, Y. Zhai, X. Zhang, E. Zhang, H. Wang, X. Liu, F. Xu, S. Kaskel, *Adv. Energy Mater.* **2021**, *11*, 2100856; b) H. He, D. Huang, Y. Tang, Q. Wang, X. Ji, H. Wang, Z. Guo, *Nano Energy* **2019**, *57*, 728–736; c) B. Cao, Q. Zhang, H. Liu, B. Xu, S. Zhang, T. Zhou, J. Mao, W. K. Pang, Z. Guo, A. Li, J. Zhou, X. Chen, H. Song, *Adv. Energy Mater.* **2018**, *8*, 1801149; d) Q. Li, J. Zhang, L. Zhong, F. Geng, Y. Tao, C. Geng, S. Li, B. Hu, Q. H. Yang, *Adv. Energy Mater.* **2022**, *12*, 2201734.
[24] J. Asenbauer, T. Eisenmann, M. Kuenzel, A. Kazzazi, Z. Chen, D. Bresser, *Sustain. Energy Fuels* **2020**, *4*, 5387–5416.
[25] J. M. Stratford, A. K. Kleppe, D. S. Keeble, P. A. Chater, S. S. Meysami, C. J. Wright, J. Barker, M. M. Titirici, P. K. Allan, C. P. Grey, *J. Am. Chem. Soc.* **2021**, *143*, 14274–14286.
[26] X. Tang, F. Xie, Y. Lu, H. Mao, Z. Chen, H. Pan, S. Weng, Y. Yang, X. Li, Z. Guo, *ACS Energy Lett.* **2024**, *9*, 1158–1167.
[27] F. Xie, Z. Xu, Z. Guo, A. C. S. Jensen, J. Feng, H. Luo, F. Ding, Y. Lu, Y. S. Hu, M. M. Titirici, *Carbon Energy* **2022**, *4*, 914–923.
[28] Y. Wan, Y. Liu, D. Chao, W. Li, D. Zhao, *Nano Materials Science* **2023**, *5*, 189–201.
[29] Z. Zeng, V. Murugesan, K. S. Han, X. Jiang, Y. Cao, L. Xiao, X. Ai, H. Yang, J.-G. Zhang, M. L. Sushko, *Nat. Energy* **2018**, *3*, 674–681.
[30] X. Zhang, X. Rui, D. Chen, H. Tan, D. Yang, S. Huang, Y. Yu, *Nanoscale* **2019**, *11*, 2556–2576.
[31] L. Yan, G. Zhang, J. Wang, Q. Ren, L. Fan, B. Liu, Y. Wang, W. Lei, D. Ruan, Q. Zhang, Z. Shi, *Energy Environ. Mater.* **2022**, *6*, e12523.
[32] G. Towler, R. Sinnott, Chemical Engineering Design: Principles, Practice and Economics of Plant and Process Design, 3rd ed., Butterworth-Heinemann: Oxford, **2021**.

Manuscript received: June 28, 2024
Revised manuscript received: August 9, 2024
Accepted manuscript online: August 14, 2024
Version of record online: October 17, 2024